ACS Catalysis

Research Article

Cite This: ACS Catal. 2018, 8, 11815−11821

pubs.acs.org/acscatalysis

Selective Photocatalytic CO_2 Reduction in Water by Electrostatic Assembly of CdS Nanocrystals with a Dinuclear Cobalt Catalyst

Qian-Qian Bi,[†] Jia-Wei Wang,[†] Jia-Xin Lv, Juan Wang, Wen Zhang,* and Tong-Bu Lu*

Institute for New Energy Materials and Low Carbon Technologies, School of Materials Science and Engineering, Tianjin University of Technology, Tianjin 300384, China

Supporting Information

ABSTRACT: In the photocatalytic conversion of CO_2 to valuable chemicals under aqueous conditions, the selectivity and the product yield still present the most challenging issues. Against this backdrop, negatively charged water-soluble CdS nanocrystals were used to assemble with a positively charged dinuclear cobalt complex through electrostatic interactions. This assembly efficiently catalyzes the CO_2-to-CO conversion under visible light, with a high selectivity of 95%, a high yield of 34.51 μmol of CO, and a large turnover number (TON) of 1380 based on the cobalt catalyst, all of which are record high values for a noble-metal-free visible-light-driven CO_2 reduction system with a molecular catalyst in a fully aqueous medium.

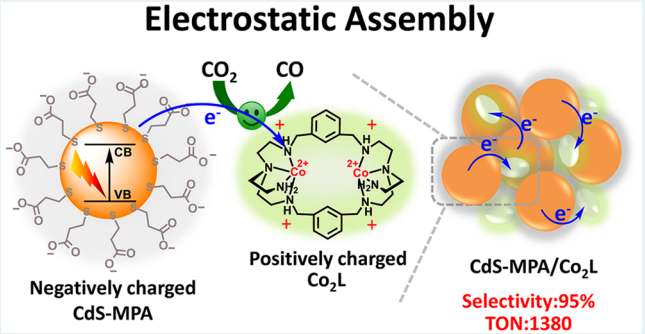

KEYWORDS: *photocatalysis, CO_2 reduction, CdS nanocrystals, dinuclear cobalt complex, electrostatic assembly*

INTRODUCTION

The construction of effective catalytic systems to convert CO_2 into value-added chemicals is an important method to reduce both the depletion of fossil fuels and the intensification of global warming.[1−8] Specifically, CO_2 reduction solely driven by solar energy is regarded as one of the most applicable techniques.[5,9−12] In this context, various metal complexes, based on Re,[13,14] Ru,[5,15] Ir,[16] Co,[17,18] Ni,[19,20] Mn,[21,22] Fe,[23−26] etc., have been developed as molecular catalysts to reduce CO_2 to CO. For solar energy to drive their catalysis, the photosensitizers, such as $[Ru(bpy)_3]Cl_2$ (bpy = 2,2′-bipyridine), $[Ir(ppy)_3](PF_6)_2$ (ppy = 2-phenylpyridine), etc., or organic dyes,[27−29] are indispensable. However, the applications of these molecular photosensitizers are restricted by several disadvantages, such as the use of precious metals, the narrow range of visible-light absorbance, and the severe photodegradation, etc.[30] In addition, most of these molecular photocatalytic reactions need to run in organic solvents rather than pure water, because of the competitive hydrogen evolution reaction in water, resulting in low CO_2 reduction selectivity.[31,32]

In contrast to molecular photosensitizers, semiconducting nanocrystals (NCs) are attractive photosensitizers, due to their large extinction coefficients, tunable redox potentials, and optical properties through regulation of particle sizes.[33] Moreover, their large specific surface areas and highly modifiable surface ligands enable their sufficient interactions with the cocatalysts, which can circumvent the low-probability bimolecular collision[34,35] and thus facilitate the electron transfer from NCs to cocatalysts.[36−38]

Despite these appealing features, however, their activity for catalytic proton reduction in aqueous medium[39−42] hinders their applications in photocatalytic CO_2 reduction systems. Thus, the related examples with high selectivity and activity are rare. In early times, CdS NCs were used as photosensitizers to cooperate with a carbon monoxide dehydrogenase for light-driven CO_2 reduction.[43] Then, Weiss and co-workers combined $CuInS_2$/ZnS NCs and an iron(III) tetraphenylporphyrin (FeTPP)[44] or a trimethylamine-functionalized iron tetraphenylporphyrin (FeTMA)[45] to achieve high selectivity (over 99%) for photocatalytic CO_2-to-CO conversion in dimethyl sulfoxide (DMSO) and water, respectively. However, both of the amounts of evolved CO in the two systems were very low (<1 μmol). A more impressive example was reported by Reisner and co-workers; they covalently immobilized a thiol-derived nickel-terpyridine complex (Ni-tpyS) on CdS NCs. The hybrid photocatalyst could reduce CO_2 to CO with a high selectivity (>90%) just at the initial stage of the reaction, while its selectivity to CO continuously decreased as the reaction progressed, because of the loss of Ni-tpyS from the NC surface, and the CO yield was still modest (≈4 μmol).[46]

In this context, the development of a higher-performance photocatalytic CO_2 reduction system with semiconducting nanocrystals is greatly desired. In our previous work,[17] a dinuclear cobalt catalyst (Co_2L' in Figure S1) displays high selectivity and efficiency for the photocatalytic reduction of

Received: August 28, 2018
Revised: October 31, 2018
Published: November 9, 2018

DOI: 10.1021/acscatal.8b03457
ACS Catal. 2018, 8, 11815−11821

Scheme 1. Illustration of CdS NCs with Different Charge Characteristics and Their Photocatalytic CO_2-to-CO Conversion

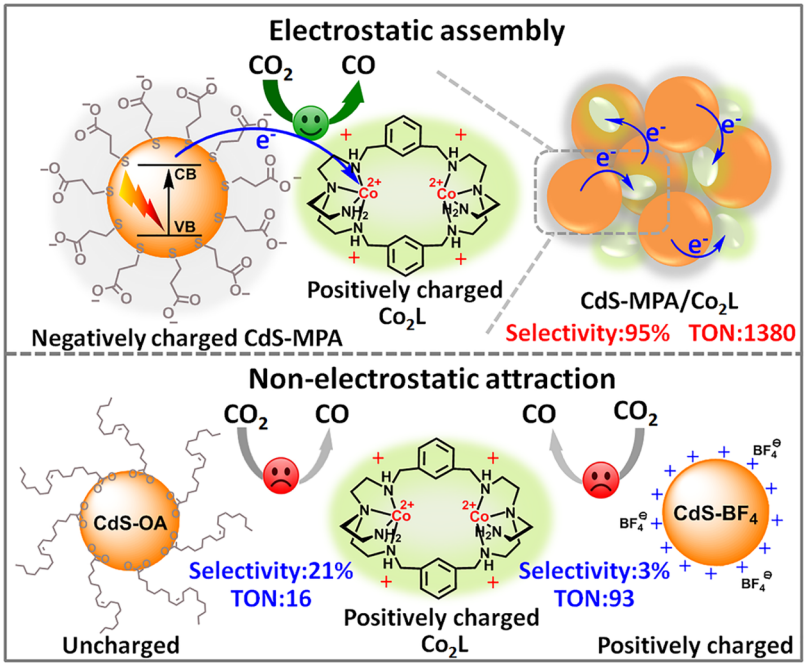

CO_2 to CO, benefiting from the synergistic effect between two cobalt ions within the catalyst. However, its performance is limited by the use of organic solvent and the precious-metal-based photosensitizer, $[Ru(phen)_3](PF_6)_2$. Against this backdrop, we designed and synthesized a new dinuclear cobalt complex (Co_2L; Scheme 1), in which a hydrophobic benzene ring in the ligand structure was removed by contrast to the previously reported Co_2L'. This feature endows the new Co_2L a higher water solubility (2.8×10^{-3} mol/L, 1.5 times higher than that of Co_2L'), as well as an easier access to capture and transform CO_2. Meanwhile, we chose CdS NCs capped with mercaptopropionic acid (MPA) as the light absorbers instead of $[Ru(phen)_3](PF_6)_2$ and found that the semiconductor is highly advantageous in terms of water solubility, photostability, and expense. Most importantly, the negatively charged CdS-MPA can form an assembly with the positively charged Co_2L through electrostatic interactions (Scheme 1). The assembly could facilitate electronic communication between the light absorbers and cocatalysts, leading to durable and selective photocatalytic CO_2-to-CO conversion even in purely aqueous solutions, with a selectivity of 95%, a remarkable yield of 34.51 μmol of CO, and a large turnover number of 1380 based on the cobalt catalyst. No decrease was observed on the CO selectivity even after 120 h of photocatalysis.

EXPERIMENTAL SECTION

Materials and Methods. Co_2L was prepared via a four-step synthetic procedure (Scheme S1). CdS NCs with different capping agents were synthesized according to the literature.[47] Their detailed synthetic procedures and basic characterization can be found in the Experimental Details section and Figures S2–S10 in the Supporting Information. Nuclear magnetic resonance (NMR) spectra were performed on a Bruker 400 MHz instrument. High-resolution mass spectra (HRMS) were recorded on a Q-TOF LC–MS instrument with an ESI mode. Ion chromatograph experiments were conducted on an ECO Mestrosep instrument with a supp 5-250 column. UV–vis absorption spectra were detected on a Lambda 750 UV/vis/NIR spectrophotometer. Infrared spectroscopy (IR) was performed on a PerkinElmer Frontier Mid-IR instrument. Inductively coupled plasma mass spectrometry (ICP-MS) was recorded on a Thermo Fisher iCAP RQ instrument. Dynamic light scattering (DLS) measurements were examined with a laser-light scattering spectrometer equipped with a digital correlator at 636 nm at a scattering angle of 90°. The $^{13}CO_2$ isotope trace experiments were detected on an Agilent 7890B/5977B GC-MS instrument. X-ray photoelectron spectroscopy (XPS) was conducted on an ESCALAB 250 Xi spectrometer (Thermo Scientific). Transmission electron microscope (TEM) measurements were characterized on a Talos F200X instrument, FEI, using 200 kV acceleration voltage. Photoluminescence (PL) spectra were recorded by a fluorescence spectrophotometer (F-7000, Hitachi, Tokyo, Japan). The time-resolved fluorescence spectra were measured by a time-resolved confocal fluorescence instrument (MicroTime 200, PicoQuant, Berlin, Germany). Mott–Schottky plots were measured by impedance-potential technique on the CHI 760E electrochemical station.

RESULTS AND DISCUSSION

Redox Properties. At the beginning, the redox properties of Co_2L and CdS NCs were investigated. Initially, the cyclic voltammogram (CV) of Co_2L in a 0.1 M $NaHCO_3$ aqueous solution under a CO_2 atmosphere suggests its electrocatalytic activity for CO_2 reduction, as an enhanced current (E_{onset} = −0.80 V vs NHE) was observed relative to the CV under argon (Figure S9). On the other side, the band gap of CdS-MPA was determined by UV–vis spectroscopy (Figure 1a). The obtained spectrum was converted to a plot of $(\alpha h\nu)^2$ versus photon energy, and the direct band gap of CdS-MPA was estimated as 2.54 eV (Figure 1b). Additionally, the flat-band potential (corresponding to the conduction band) of CdS-MPA obtained from the Mott–Schottky plots was −0.87 V vs NHE (Figure 1c). The above results indicate that the

DOI: 10.1021/acscatal.8b03457
ACS Catal. 2018, 8, 11815–11821

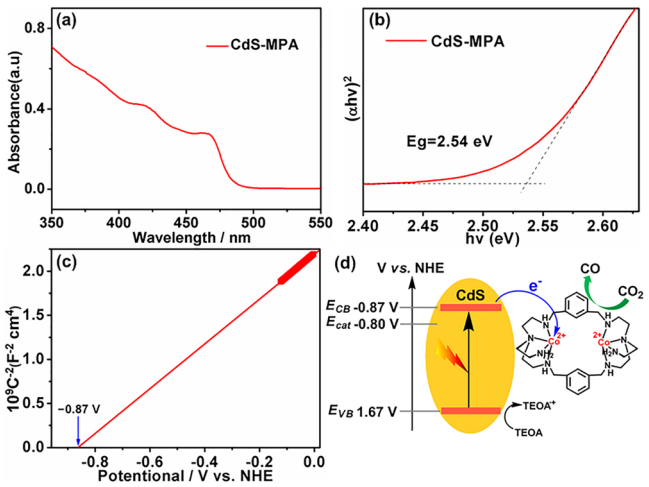

Figure 1. (a) UV−vis absorption spectra of CdS-MPA and (b) corresponding Tauc plots $(\alpha h\nu)^2$ vs photon energy ($h\nu$). (c) Mott−Schottky plots of CdS-MPA. (d) Band structure of CdS-MPA and the onset potential of Co_2L for CO_2 reduction.

photoexcited CdS-MPA has enough driving force to trigger CO_2 reduction at Co_2L (Figure 1d). Specifically, the photoexcited electrons of CdS-MPA jumped from the valence band (VB) to the conduction band (CB). As the onset potential of Co_2L (−0.80 V) was less negative than the CB potential of CdS-MPA (−0.87 V), electrons from the CB of CdS-MPA can transfer to Co_2L and reduce the cobalt complex, followed by the binding and reduction of CO_2. The catalytic mechanism of Co_2L as the catalytic center can be analogous to the one proposed for Co_2L' in our previous work[17] because of their similar structures, possibly involving the $Co^{II/I}$ reduction and a synergy between two cobalt centers.

Photocatalytic CO_2 Reduction. Encouraged by the positive information above, we screened the reaction conditions for photocatalytic CO_2 reduction using CdS-MPA as the photosensitizer and Co_2L as the cocatalyst. Photocatalytic solutions were prepared by sequentially adding stock solutions of CdS-MPA and catalyst Co_2L to aqueous solutions with a sacrificial reductant (0.3 M). The photoreactor was sealed with a rubber septum and saturated with CO_2, followed by the visible-light irradiation. First, in the presence of triethanolamine (TEOA) as a sacrificial reductant, it was observed that H_2O was a more appropriate solvent compared with CH_3CN/H_2O (v:v = 4:1) with a relatively higher selectivity and catalytic activity for CO production (Table 1, entries 1 and 2). Water not only serves as a better solvent to dissolve the negatively charged CdS/MPA, but also provides protons to facilitate the proton-dependent CO_2 reduction. The role of H_2O was also investigated with D_2O as medium (Figure S11). The total amount of CO_2 reduction products and the ratio of n_{CO}/n_{CD_4} in D_2O were both lower than those in H_2O, indicating that the protons in H_2O played an important role in the CO_2 reduction. Subsequently, we varied the sacrificial reductants (Table 1, entries 2−4) and found that the use of TEOA enabled a better performance than sodium ascorbate or sulfite, which could be attributed to the fact that TEOA is more efficient to capture the photogenerated holes from CdS. In an attempt to improve the selectivity of the photocatalytic reduction of CO_2, $NaHCO_3$ was added to the reaction system, which may buffer the solution and increase the solubility of CO_2. The results show that the TON of CO production (942) and the selectivity (95%) were simultaneously increased in the presence of $NaHCO_3$ with a small amount of methane, more intriguingly, without the trace of H_2 evolution (Table 1, entry 5).

To illustrate the function of each component in the photocatalytic system, we conducted a series of reference experiments. Using Ar instead of CO_2, negligible amounts of CO and CH_4 were detected (Table 2, entry 2). The $^{13}CO_2$ isotope trace experiment was also conducted. As shown in Figure S12, the peak with the m/z value of 29 clearly indicated the generation of ^{13}CO, revealing that CO was generated dominantly from the reduction of CO_2 instead of $NaHCO_3$ or other organic components. Additionally, as shown in Table 2 (entries 3 and 4), without illumination and CdS-MPA, no gas was generated in the system. These results indicate that the

Table 2. Results of Control Experiments for the Photocatalytic Reduction of CO_2

entry	PS	n/H_2 (μmol)	n/CO (μmol)	n/CH_4 (μmol)	selectivity to CO	TON for CO
1	CdS-MPA	0	4.71	0.24	95%	942
2[a]	CdS-MPA	0	0.06	0.05	52%	12
3[b]	CdS-MPA	0	0	0	0	0
4[c]		0	0	0	0	0
5[d]	CdS-MPA	0	0.08	0.05	58%	15
6[e]	CdS-MPA	0	0.37	0.08	82%	74
7[f]	CdS-MPA	0	1.12	0.06	95%	112
8[g]	CdS-MPA	0.79	34.51	1.01	95%	1380
9[g]	CdS-OA	1.53	0.40	0.01	21%	16
10[g]	CdS-BF_4	83.70	2.33	2.24	3%	93

[a]Entry 2: 100% Ar. [b]Entry 3: without light. [c]Entry 4: without CdS-MPA. [d]Entry 5: without TEOA. [e]Entry 6: without Co_2L; [f]Entry 7: catalyst is CoL[1] (1 μM). Reaction conditions: CdS-MPA (4 μM), Co_2L (1 μM), 5 mL aqueous solution of 0.1 M $NaHCO_3$, 22 h, 300 W Xe lamp (λ>420 nm). [g]Entries 8−10: the reaction system was expanded 5-fold. Reaction conditions: CdS-MPA (4 μM), Co_2L (1 μM), 25 mL aqueous solution of 0.1 M $NaHCO_3$, 120 h, 300 W Xe lamp (λ > 420 nm). All data deviations are below 5%.

Table 1. Screening Studies of Photocatalytic Reduction[a] of CO_2

entry	sacrificial reductant	solvent	n/H_2 (μmol)	n/CO (μmol)	n/CH_4 (μmol)	selectivity to CO	TON for CO
1	TEOA	CH_3CN/H_2O	6.50	0.70	0.01	9.8%	140
2	TEOA	H_2O	9.95	3.24	0.22	24%	648
3	sodium ascorbate	H_2O	12.00	0.15	0.02	1%	31
4	Na_2SO_3	H_2O	0	0.03	0.02	58%	6
5	TEOA	$NaHCO_3$	0	4.71	0.24	95%	942

[a]Reaction conditions: CdS-MPA (4 μM), Co_2L (1 μM), 5 mL of reaction solution (CH_3CN/H_2O = 4:1 in entry 1, 0.1 M $NaHCO_3$ aqueous solution in entry 5), sacrificial reductant (0.3 M), 22 h, 25 °C, 300 W Xe lamp (λ > 420 nm). All data deviations are below 5%.

DOI: 10.1021/acscatal.8b03457
ACS Catal. 2018, 8, 11815−11821

catalysis requires the generation of photoinduced carriers from CdS NCs. Further control experiments indicated that, without TEOA, almost no CO was produced (Table 2, entry 5). For the cocatalyst, when the photoreaction was conducted in the absence of Co_2L, CO and CH_4 were also detected (Table 2, entry 6), but at a much lower production than the one with Co_2L; this outcome highlights the key role of Co_2L as the cocatalyst. All of the above results reveal that CO_2, visible light, CdS NCs, sacrificial reductant, and Co_2L are all essential for the significant generation of CO. We also investigated the importance of the dinuclear ligand in Co_2L; as seen from entry 7, when the catalyst was substituted with the corresponding mononuclear cobalt complex, CoL^1 (Figure S1), the production of CO was reduced dramatically. These data strongly indicate that the dinuclear configuration in Co_2L is more advantageous in the photocatalysis. Moreover, when the scale of the photocatalytic reaction was increased 5 times relative to that of entry 1 under the same visible light, a trace amount of formate was detected by ion chromatograph (IC) in the liquid phase (Figure S13), while the amounts of CO produced reached 34.5 μmol (TON 1380), and the selectivity also remained as high as 95% (Table 2, entry 8, and Figure S17), indicating that this photocatalytic system has potential for large-scale applications.

To explore the mechanism of reducing CO_2 to CH_4, we purged CO instead of CO_2 into the photoreaction system. The result in Figure S14 (red line) shows that CH_4 could also be produced constantly under CO atmosphere. Here, we speculate that CO may act as an intermediate to motivate the generation of CH_4. Moreover, the conversion of CO_2 to the products (CO, CH_4, and HCOOH) was detected to be 93.3% (Figure S15 and Table S1), indicating that a rough carbon balance was realized in the photocatalytic system.

Assembly Formation via Electrostatic Attraction. As depicted in Scheme 1, the self-assembly between CdS-MPA and Co_2L is likely to be driven by electrostatic attraction between the negatively charged carboxylate groups of CdS-MPA and the positively charged cobalt(II) center of Co_2L. For comparison, uncharged CdS NCs which are capped with oleic acid ligands (CdS-OA), and positively charged, surface-ligand-free NCs (CdS-BF_4), were used in parallel investigations on the influence of different surface charges on photocatalysis (Table 2, entries 8−10 and Figure 2a). The results show that, in terms of CO production, CdS-MPA was over 86 and 15 times more active than CdS-OA and CdS-BF_4, respectively. Meanwhile, the catalytic selectivity of CdS-MPA toward CO formation was much higher than those of CdS-OA and CdS-BF_4. Particularly, the H_2 yield of CdS-BF_4 was relatively high, which can be ascribed to the electrostatic repulsion between CdS-BF_4 and catalyst Co_2L. That is, the photoexcited electrons at the surface of CdS tend to react with H^+ to generate hydrogen, rather than the injection to the cocatalyst. The comparative study reveals that the electrostatic attraction between the negatively charged CdS NCs and the positively charged catalyst Co_2L plays a key role in achieving the high performance for photocatalytic CO_2 reduction.

The overall time profile of the photocatalytic CO_2 reduction is shown in Figure S17. CO was the main reduction product (34.5 μmol) during the photocatalysis along with a small amount of CH_4 (1.0 μmol). Interestingly, the CO production was lethargic in the first 5 h (Figure 2b, black line). Then, the rate of CO production abruptly increased after 5 h, followed by the slackened and finally ceased reaction. This phenomenon

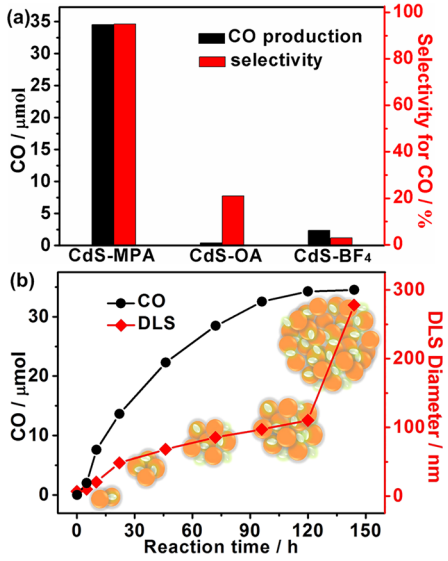

Figure 2. (a) CO production and selectivity of CdS-MPA, CdS-OA, and CdS-BF_4. (b) Time profiles of DLS data and photocatalytic CO evolution. Reaction conditions: CdS-MPA (4 μM), Co_2L (1 μM), 25 mL aqueous solution of 0.1 M $NaHCO_3$, 25 °C, 300 W Xe lamp (λ > 420 nm).

can be explained by the possibility that, at the initial stage of the reaction, the formation of the assembly is insufficient and cannot readily facilitate the electron transfer between CdS and Co_2L. For a confirmation of this speculation, DLS measurements were employed to track the changes of the assembly size during the photocatalytic reaction (Figure 2b, red line, and Figure S16). It was observed that the diameter of the assembly in the initial 5 h (10.1 nm) was close to that of individual CdS NCs (7.1 nm) (Figure S16a), indicating that the assembling of Co_2L and NCs was not marked at the initial stage. When the reaction proceeded for 10 h, the detected diameter reached 20.6 nm, suggesting a more substantial formation of the assembly, concomitant with a drastically increased CO production. Upon further reaction, the size of the assembly kept increasing up to 278.0 nm, while the rate of CO production slowed down and eventually ceased after 120 h. This observation is attributed to the overassembly that could impede the mass transfer, which can be viewed by the TEM image (Figure 3a) of the centrifuged mixture after photoreaction. In addition, the isolated precipitation of CdS-MPA/Co_2L was reused to catalyze the CO_2 conversion. The evolution of CO was obviously lower compared with the one in the first run (Figure S20), indicating that the overgrowth of the CdS-MPA assembly will impair the photocatalytic performance of the CdS-MPA/Co_2L assembly. However, the excessive aggregation had no impact on the high selectivity to CO (95%) that could be maintained for 120 h. Such retention of selectivity is distinguished from the case of Ni-tpyS anchored on CdS NCs, where the dissociation of Ni-tpyS from the CdS surface diminished the CO selectivity.[46] This difference suggests the firm combination between CdS NCs and Co_2L cocatalyst during long-term photocatalysis.

A series of experiments were deliberately carried out on the isolated solid from the centrifugation of the reaction mixture to further verify the assembling between CdS-MPA and the cocatalyst Co_2L. First, inductively coupled plasma mass spectrometry (ICP-MS; Figure S18) shows that cobalt element actually exists, and the mass content of Co is measured as

DOI: 10.1021/acscatal.8b03457
ACS Catal. 2018, 8, 11815−11821

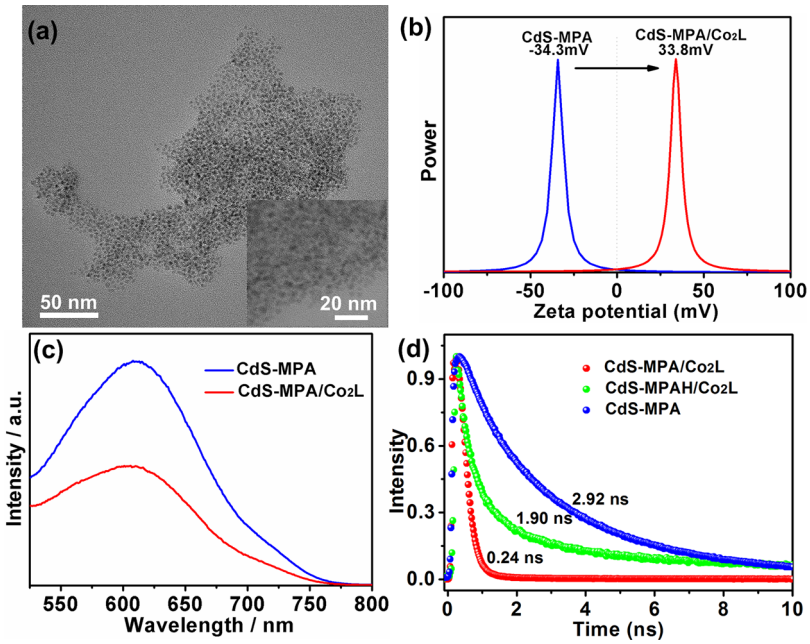

Figure 3. (a) TEM image of centrifugal mixture after photoreaction (inset: corresponding high-resolution TEM, HRTEM, image). (b) ζ potentials of CdS-MPA (blue line) and CdS-MPA/Co_2L (red line). (c) PL emission spectra (the excitation wavelength is 420 nm). (d) PL decay of CdS-MPA without (black) and with (red) added Co_2L and CdS-MPAH with added Co_2L (green) obtained by placing a long-pass optical filter (519 nm) before the detector, after excitation at 439 nm.

0.053 ± 0.005%. Then, the liquid chromatography−mass spectrometry (LC−MS) of the ultrasonic dispersed solid from the centrifugation of the reaction mixture is measured (Figure S19). The peaks at 401.13, 337.20, and 420.13 represent $[Co_2L(ClO_4^-)(HCOO^-)CO_2]^{2+}$, $[Co_2L(CO_3^{2-})]^{2+}$, and $Co_2L(ClO_4^-)(HCOO^-)(CH_3CN)_2]^{2+}$, respectively, indicating the integration of the molecular catalyst Co_2L with the CdS NCs. The comparison of IR spectra between this solid and Co_2L further demonstrates that the assembly isolated from the reaction mixture contains a substantial amount of Co_2L (Figure S21). Moreover, the measurements of ζ potential provide additional evidence on the formation of the assembly. For the aqueous solution of CdS-MPA, the ζ potential was measured as −34.3 mV (Figure 3b), demonstrating a negatively charged nature of the NCs surface. In contrast, the ζ potential of the centrifuged precipitate after photoreaction was determined as +33.8 mV; the reversed polarity confirms the electrostatic assembly between the negatively charged CdS-MPA and the positively charged Co_2L. PXRD measurements (Figure S22) and the XPS spectra (Figure S23) of the isolated solid CdS-MPA/Co_2L after CO_2 reduction had similar peaks as the original CdS-MPA and the mixture of CdS-MPA and Co_2L before CO_2 reduction, indicating that CdS-MPA can maintain its crystal structure and composition before and after the reaction. All of these results confirm that, through electrostatic interactions, the photosensitizing CdS NCs can be assembled with Co_2L as the cocatalyst in the photocatalytic CO_2 reduction, and it has been demonstrated that this integration remarkably promotes the electron transfer between them. Moreover, the stability of nonassembled Co_2L in the reaction was confirmed by XPS and ESI-MS measurements via adding excess Co_2L to the reaction system (Figures S24 and S25).

With the confirmation of the formation of the photosensitizer−catalyst assembly, it can be anticipated that this assembling is likely to achieve a fast photogenerated electron transfer between them. This anticipation was examined by PL measurements. As exhibited in Figure 3c,d, in the presence of 2.0 equiv of Co_2L, the photoexcited emission of CdS-MPA at 610 nm was obviously quenched, and simultaneously the emission lifetime of CdS-MPA dramatically decreased from 2.92 to 0.24 ns. For comparison, the negatively charged carboxylate groups of CdS-MPA were protonated and converted into carboxylic groups, with the sampled named as CdS-MPAH (characterized by ζ potentials in Figure S26), which was employed to check whether the electrostatic interactions between CdS-MPAH and Co_2L were restrained. Finally, the emission lifetime of protonated CdS-MPAH was measured as 1.90 ns, which is much larger than the fluorescence lifetime of intact CdS-MPA with Co_2L. These observations indicate that, with the participation of electrostatic attraction, a faster transfer of photogenerated electrons from CdS NCs to Co_2L can be achieved. These findings also highlight that the noncovalent assembly between CdS NCs and molecular cocatalyst can be an advisable strategy to enable fast electron transfer between catalysts and photosensitizers.

■ CONCLUSIONS

In summary, we constructed a photocatalytic assembly via electrostatic interactions between negatively charged CdS NCs and a positively charged dinuclear cobalt catalyst. The photocatalytic reduction of CO_2 to CO with this assembly can accomplish record high CO yield (34.51 μmol), TON (1380), and selectivity (95%) in terms of NC-mediated photocatalytic CO_2 reduction in an aqueous solution (see Table S2). In sharp contrast, the parallel experiments with electrically neutral (CdS-OA, TON 16, selectivity 21%) and positively charged (CdS-BF_4, TON 93, selectivity 3%) NCs both exhibited much lower activity and selectivity for photocatalytic CO_2 reduction. Corroborated with the results of PL experiments, we have shown that such simple

DOI: 10.1021/acscatal.8b03457
ACS Catal. 2018, 8, 11815−11821

noncovalent interactions, without the assistance of an elaborate synthetic process, successfully accelerate the electron transfer between the photosensitizers and the molecular catalysts. We believe that the noncovalent assembly of photocatalytic active species could not only provide a convenient method to construct an efficient artificial photosynthetic system but also expand the possible applications of ultrafine NCs in photocatalytic reactions which require multielectron injection.

■ ASSOCIATED CONTENT

Supporting Information

The Supporting Information is available free of charge on the ACS Publications website at DOI: 10.1021/acscatal.8b03457.

Synthesis route and characterization of Co_2L, CdS-MPA, CdS-OA, and CdS-BF_4, including the results of NMR, HRMS (ESI), electrochemistry, ICP-MS, TEM, DLS, XPS, and IR (PDF)

■ AUTHOR INFORMATION

Corresponding Authors

*E-mail: zhangwen@email.tjut.edu.cn.
*E-mail: lutongbu@mail.sysu.edu.cn.

ORCID

Wen Zhang: 0000-0001-6105-3286
Tong-Bu Lu: 0000-0002-6087-4880

Author Contributions

†Q.-Q.B. and J.-W.W. contributed equally.

Notes

The authors declare no competing financial interest.

■ ACKNOWLEDGMENTS

This work was financially supported by National Key R&D Program of China (2017YFA0700104) and NSFC (21331007, 21790052, and 21702146).

■ REFERENCES

(1) Arai, T.; Sato, S.; Morikawa, T. A Monolithic Device for CO_2 Photoreduction to Generate Liquid Organic Substances in a Single-Compartment Reactor. *Energy Environ. Sci.* **2015**, *8*, 1998−2002.

(2) Ishida, H.; Tanaka, K.; Tanaka, T. Electrochemical CO_2 Reduction Catalyzed by Ruthenium Complexes $[Ru(bpy)_2(CO)_2]^{2+}$ and $[Ru(bpy)_2(CO)Cl]^+$. Effect of pH on the Formation of CO and HCOO. *Organometallics* **1987**, *6*, 181−186.

(3) Iwase, A.; Yoshino, S.; Takayama, T.; Ng, Y. H.; Amal, R.; Kudo, A. Water Splitting and CO_2 Reduction under Visible Light Irradiation Using Z-Scheme Systems Consisting of Metal Sulfides, CoO_x-Loaded $BiVO_4$, and a Reduced Graphene Oxide Electron Mediator. *J. Am. Chem. Soc.* **2016**, *138*, 10260−10264.

(4) Kuramochi, Y.; Itabashi, J.; Fukaya, K.; Enomoto, A.; Yoshida, M.; Ishida, H. Unexpected Effect of Catalyst Concentration on Photochemical CO_2 Reduction by Trans(Cl)-Ru(bpy)$(CO)_2Cl_2$: New Mechanistic Insight into the $CO/HCOO^-$ Selectivity. *Chem. Sci.* **2015**, *6*, 3063−3074.

(5) Kuriki, R.; Matsunaga, H.; Nakashima, T.; Wada, K.; Yamakata, A.; Ishitani, O.; Maeda, K. Nature-Inspired, Highly Durable CO_2 Reduction System Consisting of a Binuclear Ruthenium(II) Complex and an Organic Semiconductor Using Visible Light. *J. Am. Chem. Soc.* **2016**, *138*, 5159−5170.

(6) Langer, R.; Diskin-Posner, Y.; Leitus, G.; Shimon, L. J.; Ben-David, Y.; Milstein, D. Low-Pressure Hydrogenation of Carbon Dioxide Catalyzed by an Iron Pincer Complex Exhibiting Noble Metal Activity. *Angew. Chem., Int. Ed.* **2011**, *50*, 9948−9952.

(7) Sahara, G.; Kumagai, H.; Maeda, K.; Kaeffer, N.; Artero, V.; Higashi, M.; Abe, R.; Ishitani, O. Photoelectrochemical Reduction of CO_2 Coupled to Water Oxidation Using a Photocathode with a Ru(II)−Re(I) Complex Photocatalyst and a CoOx/TaON Photoanode. *J. Am. Chem. Soc.* **2016**, *138*, 14152−14158.

(8) Schreier, M.; Curvat, L.; Giordano, F.; Steier, L.; Abate, A.; Zakeeruddin, S. M.; Luo, J.; Mayer, M. T.; Grätzel, M. Efficient Photosynthesis of Carbon Monoxide from CO_2 Using Perovskite Photovoltaics. *Nat. Commun.* **2015**, *6*, 7326.

(9) Gao, C.; Meng, Q.; Zhao, K.; Yin, H.; Wang, D.; Guo, J.; Zhao, S.; Chang, L.; He, M.; Li, Q.; Zhao, H.; Huang, X.; Gao, Y.; Tang, Z. Co_3O_4 Hexagonal Platelets with Controllable Facets Enabling Highly Efficient Visible-Light Photocatalytic Reduction of CO_2. *Adv. Mater.* **2016**, *28*, 6485−6490.

(10) Froehlich, J. D.; Kubiak, C. P. The Homogeneous Reduction of CO_2 by $[Ni(Cyclam)]^+$: Increased Catalytic Rates with the Addition of a CO Scavenger. *J. Am. Chem. Soc.* **2015**, *137*, 3565−3573.

(11) Nakajima, T.; Tamaki, Y.; Ueno, K.; Kato, E.; Nishikawa, T.; Ohkubo, K.; Yamazaki, Y.; Morimoto, T.; Ishitani, O. Photocatalytic Reduction of Low Concentration of CO_2. *J. Am. Chem. Soc.* **2016**, *138*, 13818−13821.

(12) Olah, G. A.; Goeppert, A.; Prakash, G. K. S. Chemical Recycling of Carbon Dioxide to Methanol and Dimethyl Ether: From Greenhouse Gas to Renewable, Environmentally Carbon Neutral Fuels and Synthetic Hydrocarbons. *J. Org. Chem.* **2009**, *74*, 487−498.

(13) Morimoto, T.; Nakajima, T.; Sawa, S.; Nakanishi, R.; Imori, D.; Ishitani, O. CO_2 Capture by a Rhenium(I) Complex with the Aid of Triethanolamine. *J. Am. Chem. Soc.* **2013**, *135*, 16825−16828.

(14) Morimoto, T.; Nishiura, C.; Tanaka, M.; Rohacova, J.; Nakagawa, Y.; Funada, Y.; Koike, K.; Yamamoto, Y.; Shishido, S.; Kojima, T.; Saeki, T.; Ozeki, T.; Ishitani, O. Ring-Shaped Re(I) Multinuclear Complexes with Unique Photofunctional Properties. *J. Am. Chem. Soc.* **2013**, *135*, 13266−13269.

(15) Kuriki, R.; Yamamoto, M.; Higuchi, K.; Yamamoto, Y.; Akatsuka, M.; Lu, D.; Yagi, S.; Yoshida, T.; Ishitani, O.; Maeda, K. Robust Binding between Carbon Nitride Nanosheets and a Binuclear Ruthenium(II) Complex Enabling Durable, Selective CO_2 Reduction under Visible Light in Aqueous Solution. *Angew. Chem., Int. Ed.* **2017**, *56*, 4867−4871.

(16) Sato, S.; Morikawa, T.; Kajino, T.; Ishitani, O. A Highly Efficient Mononuclear Iridium Complex Photocatalyst for CO_2 Reduction under Visible Light. *Angew. Chem., Int. Ed.* **2013**, *52*, 988−992.

(17) Ouyang, T.; Huang, H. H.; Wang, J. W.; Zhong, D. C.; Lu, T. B. A Dinuclear Cobalt Cryptate as a Homogeneous Photocatalyst for Highly Selective and Efficient Visible-Light Driven CO_2 Reduction to CO in CH_3CN/H_2O Solution. *Angew. Chem., Int. Ed.* **2017**, *56*, 738−743.

(18) Guo, Z.; Cheng, S.; Cometto, C.; Anxolabehere-Mallart, E.; Ng, S. M.; Ko, C. C.; Liu, G.; Chen, L.; Robert, M.; Lau, T. C. Highly Efficient and Selective Photocatalytic CO_2 Reduction by Iron and Cobalt Quaterpyridine Complexes. *J. Am. Chem. Soc.* **2016**, *138*, 9413−9416.

(19) Thoi, V. S.; Kornienko, N.; Margarit, C. G.; Yang, P.; Chang, C. J. Visible-Light Photoredox Catalysis: Selective Reduction of Carbon Dioxide to Carbon Monoxide by a Nickel N-Heterocyclic Carbene-Isoquinoline Complex. *J. Am. Chem. Soc.* **2013**, *135*, 14413−14424.

(20) Zhao, C.; Dai, X.; Yao, T.; Chen, W.; Wang, X.; Wang, J.; Yang, J.; Wei, S.; Wu, Y.; Li, Y. Ionic Exchange of Metal−Organic Frameworks to Access Single Nickel Sites for Efficient Electroreduction of CO_2. *J. Am. Chem. Soc.* **2017**, *139*, 8078−8081.

(21) Torralba-Peñalver, E.; Luo, Y.; Compain, J.-D.; Chardon-Noblat, S.; Fabre, B. Selective Catalytic Electroreduction of CO_2 at Silicon Nanowires (SiNWs) Photocathodes Using Non-Noble Metal-Based Manganese Carbonyl Bipyridyl Molecular Catalysts in Solution and Grafted onto SiNWs. *ACS Catal.* **2015**, *5*, 6138−6147.

(22) Takeda, H.; Koizumi, H.; Okamoto, K.; Ishitani, O. Photocatalytic CO_2 Reduction Using a Mn Complex as a Catalyst. *Chem. Commun.* **2014**, *50*, 1491−1493.

(23) Takeda, H.; Ohashi, K.; Sekine, A.; Ishitani, O. Photocatalytic CO_2 Reduction Using Cu(I) Photosensitizers with a Fe(II) Catalyst. *J. Am. Chem. Soc.* **2016**, *138*, 4354−4357.
(24) Alsabeh, P. G.; Rosas-Hernandez, A.; Barsch, E.; Junge, H.; Ludwig, R.; Beller, M. Iron-Catalyzed Photoreduction of Carbon Dioxide to Synthesis Gas. *Catal. Sci. Technol.* **2016**, *6*, 3623−3630.
(25) Bonin, J.; Robert, M.; Routier, M. Selective and Efficient Photocatalytic CO_2 Reduction to CO Using Visible Light and an Iron-Based Homogeneous Catalyst. *J. Am. Chem. Soc.* **2014**, *136*, 16768−16771.
(26) Cometto, C.; Kuriki, R.; Chen, L.; Maeda, K.; Lau, T.-C.; Ishitani, O.; Robert, M. A Carbon Nitride/Fe Quaterpyridine Catalytic System for Photostimulated CO_2-to-CO Conversion with Visible Light. *J. Am. Chem. Soc.* **2018**, *140*, 7437−7440.
(27) Takeda, H.; Cometto, C.; Ishitani, O.; Robert, M. Electrons, Photons, Protons and Earth-Abundant Metal Complexes for Molecular Catalysis of CO_2 Reduction. *ACS Catal.* **2017**, *7*, 70−88.
(28) Arias-Rotondo, D. M.; McCusker, J. K. The Photophysics of Photoredox Catalysis: A Roadmap for Catalyst Design. *Chem. Soc. Rev.* **2016**, *45*, 5803−5820.
(29) Kumar, B.; Llorente, M.; Froehlich, J.; Dang, T.; Sathrum, A.; Kubiak, C. P. Photochemical and Photoelectrochemical Reduction of CO_2. *Annu. Rev. Phys. Chem.* **2012**, *63*, 541−569.
(30) Boston, D. J.; Xu, C.; Armstrong, D. W.; MacDonnell, F. M. Photochemical Reduction of Carbon Dioxide to Methanol and Formate in a Homogeneous System with Pyridinium Catalysts. *J. Am. Chem. Soc.* **2013**, *135*, 16252−16255.
(31) White, J. L.; Baruch, M. F.; Pander, J. E.; Hu, Y.; Fortmeyer, I. C.; Park, J. E.; Zhang, T.; Liao, K.; Gu, J.; Yan, Y.; Shaw, T. W.; Abelev, E.; Bocarsly, A. B. Light-Driven Heterogeneous Reduction of Carbon Dioxide: Photocatalysts and Photoelectrodes. *Chem. Rev.* **2015**, *115*, 12888−12935.
(32) Zheng, M.; Cao, X.; Ding, Y.; Tian, T.; Lin, J. Boosting Photocatalytic Water Oxidation Achieved by $BiVO_4$ Coupled with Iron-Containing Polyoxometalate: Analysis the True Catalyst. *J. Catal.* **2018**, *363*, 109−116.
(33) Yu, W. W.; Qu, L.; Guo, W.; Peng, X. Experimental Determination of the Extinction Coefficient of CdTe, CdSe, and CdS Nanocrystals. *Chem. Mater.* **2003**, *15*, 2854−2860.
(34) Brown, K. A.; Wilker, M. B.; Boehm, M.; Dukovic, G.; King, P. W. Characterization of Photochemical Processes for H_2 Production by CdS Nanorod−[FeFe] Hydrogenase Complexes. *J. Am. Chem. Soc.* **2012**, *134*, 5627−5636.
(35) Knowles, K. E.; Malicki, M.; Weiss, E. A. Dual-Time Scale Photoinduced Electron Transfer from PbS Quantum Dots to a Molecular Acceptor. *J. Am. Chem. Soc.* **2012**, *134*, 12470−12473.
(36) Amirav, L.; Alivisatos, A. P. Photocatalytic Hydrogen Production with Tunable Nanorod Heterostructures. *J. Phys. Chem. Lett.* **2010**, *1*, 1051−1054.
(37) Brown, K. A.; Dayal, S.; Ai, X.; Rumbles, G.; King, P. W. Controlled Assembly of Hydrogenase-CdTe Nanocrystal Hybrids for Solar Hydrogen Production. *J. Am. Chem. Soc.* **2010**, *132*, 9672−9680.
(38) Yu, W. W.; Peng, X. Formation of High-Quality CdS and Other II-VI Semiconductor Nanocrystals in Noncoordinating Solvents: Tunable Reactivity of Monomers. *Angew. Chem.* **2007**, *119*, 2611−2611.
(39) Han, Z.; Eisenberg, R. Fuel from Water: The Photochemical Generation of Hydrogen from Water. *Acc. Chem. Res.* **2014**, *47*, 2537−2544.
(40) Li, X. B.; Gao, Y. J.; Wang, Y.; Zhan, F.; Zhang, X. Y.; Kong, Q. Y.; Zhao, N. J.; Guo, Q.; Wu, H. L.; Li, Z. J.; Tao, Y.; Zhang, J. P.; Chen, B.; Tung, C. H.; Wu, L. Z. Self-Assembled Framework Enhances Electronic Communication of Ultrasmall-Sized Nanoparticles for Exceptional Solar Hydrogen Evolution. *J. Am. Chem. Soc.* **2017**, *139*, 4789−4796.
(41) Wu, L. Z.; Chen, B.; Li, Z. J.; Tung, C. H. Enhancement of the Efficiency of Photocatalytic Reduction of Protons to Hydrogen Via Molecular Assembly. *Acc. Chem. Res.* **2014**, *47*, 2177−2185.
(42) Han, Z.; Qiu, F.; Eisenberg, R.; Holland, P. L.; Krauss, T. D. Robust Photogeneration of H_2 in Water Using Semiconductor Nanocrystals and a Nickel Catalyst. *Science* **2012**, *338*, 1321.
(43) Chaudhary, Y. S.; Woolerton, T. W.; Allen, C. S.; Warner, J. H.; Pierce, E.; Ragsdale, S. W.; Armstrong, F. A. Visible Light-Driven CO_2 Reduction by Enzyme Coupled CdS Nanocrystals. *Chem. Commun.* **2012**, *48*, 58−60.
(44) Lian, S.; Kodaimati, M. S.; Dolzhnikov, D. S.; Calzada, R.; Weiss, E. A. Powering a CO_2 Reduction Catalyst with Visible Light through Multiple Sub-Picosecond Electron Transfers from a Quantum Dot. *J. Am. Chem. Soc.* **2017**, *139*, 8931−8938.
(45) Lian, S.; Kodaimati, M. S.; Weiss, E. A. Photocatalytically Active Superstructures of Quantum Dots and Iron Porphyrins for Reduction of CO_2 to CO in Water. *ACS Nano* **2018**, *12*, 568−575.
(46) Kuehnel, M. F.; Orchard, K. L.; Dalle, K. E.; Reisner, E. Selective Photocatalytic CO_2 Reduction in Water through Anchoring of a Molecular Ni Catalyst on CdS Nanocrystals. *J. Am. Chem. Soc.* **2017**, *139*, 7217−7223.
(47) Chang, C. M.; Orchard, K. L.; Martindale, B. C. M.; Reisner, E. Ligand Removal from CdS Quantum Dots for Enhanced Photocatalytic H_2 Generation in pH Neutral Water. *J. Mater. Chem. A* **2016**, *4*, 2856−2862.

DOI: 10.1021/acscatal.8b03457
ACS Catal. 2018, 8, 11815−11821